Part 7
Discontinuous Galerkin Methods

Local Time-stepping for Explicit Discontinuous Galerkin Schemes

Gregor Gassner, Michael Dumbser, Florian Hindenlang and Claus-Dieter Munz

Abstract A class of explicit discontinuous Galerkin schemes is described which time approximation is based on a predictor corrector formulation. The approximation at the new time level is obtained in one step with use of the information from the direct neighbors only. This allows to introduce a local time-stepping for unsteady simulations with the property that every grid cell runs with its own optimal time step.

1 Introduction

The time discretization in discontinuous Galerkin schemes for advection diffusion reaction equations is often based on the so called ODE (Ordinary Differential Equation) or method of lines approach. In this approach the discretization in space is applied first and then the time discretization is applied in a second step using an ODE solver. The attractivity is that the space and time discretization separates which simplifies the structure and gives latitude to change time and space approximation independently. In this paper, we describe an explicit time approximation which may be considered as a formulation in the space-time domain rather than in a separate step. The numerical scheme is kept explicit by a predictor corrector approach.

Such an approach was first proposed within the finite volume framework. The second order accurate MUSCL scheme has this form which was generalized by Harten et al. [4] in their famous paper about ENO schemes. Here, a truncated Taylor expansion in time is used to predict the time evolution of the data within the grid cell. The time derivatives are successively replaced by space derivatives using the evolution equation, usually called the Cauchy Kovalewskaya procedure.

Gregor Gassner, Michael Dumbser, Florian Hindenlang · Claus-Dieter Munz
Institute of Aerodynamics and Gas Dynamics, Universitat Stuttgart, D70550 Stuttgart, Germany, e-mail: [gassner,dumbser,hindenlang,munz]@iag.uni-stuttgart.de

We generalize this procedure in this paper and incorporate it into the DG schemes. The Taylor expansion may be considered as a local predictor which approximates the time evolution within the grid cell. Lörcher et al. [5] proposed to use a space-time expansion in the barycenter, applying the Cauchy Kovalewskaya procedure, and used this local solution to evaluate the space-time integrals in the fully discrete DG formulation. This Taylor expansion may be replaced by any other approximate solution of the local Cauchy problem which gives a space-time approximation within the grid cell. Dumbser et al. [2, 3] proposed to use a locally implicit either continuous or discontinuous Galerkin time discretization to define an auxiliary solution. Here, we describe a novel idea using a local continuous extension Runge Kutta scheme.

This first step can be considered as a predictor that gives the needed time accurate data for the evaluation of the integrals in the discrete variational formulation. As every explicit scheme the predictor corrector approach has a time step restriction. For unsteady solutions this time step restriction is also a natural condition of consistency, because it guarantees the appropriate resolution of the solution in time, too. But it becomes cumbersome for unstructured grids with small grid cells to resolve the geometry or for solutions with different local time scales. Using a global time step, the grid cell with the smallest time step defines the time step for all grid cells. In our explicit DG approach, there is a remedy for this drop in efficiency. The locality of the explicit space-time DG scheme allows a completely new time marching technique: Each grid cell may run with its own time step in a time-consistent manner, thus local time stepping for unsteady problems.

2 General Formulation

In the following we discuss the discontinuous Galerkin method. To keep matters simple, we restrict the discussion to a scalar conservation law of the form

$$u_t + \nabla \cdot \mathbf{f} = 0, \tag{1}$$

with appropriate initial and boundary conditions in a domain $\Omega \times [0;T] \subseteq R^d \times R_0^+$. The flux function $\mathbf{f}(u,\nabla u)$ is composed of two parts

$$\mathbf{f} = \mathbf{f}(u,\nabla u) = \mathbf{f}^a(u) - \mathbf{f}^v(u,\nabla u)\,, \quad \mathbf{f}^v(u,\nabla u) = \mu(u)\nabla u. \tag{2}$$

The first step of our approximation is to subdivide the domain Ω in non-overlapping grid cells Q. For every grid cell, we use a local polynomial approximation of the form

$$u(\mathbf{x},t)\big|_Q \approx u_Q(\mathbf{x},t) = \sum_{j=1}^{N} \hat{u}_j^Q(t)\varphi_j^Q(\mathbf{x}) =: \underline{\hat{u}}^Q(t)\cdot\underline{\varphi}^Q(\mathbf{x}), \quad N = \frac{(p+d)!}{p!d!}, \tag{3}$$

where $\{\varphi_j^Q(\mathbf{x})\}_{j=1,\dots,N}$ is a set of modal hierarchical orthonormal basis functions. The dimension of this space N and thus the number of time dependent degrees of freedom $\hat{u}_j^Q(t)$ depends on the polynomial degree p and the spatial dimension d. The next step of our approximation is to define how the degrees of freedom $\hat{u}_j^Q(t)$ are determined. The base of the considered discontinuous Galerkin method is a weak formulation. We insert the approximate solution (3) into the conservation law (1), multiply with a test function $\phi = \phi(\mathbf{x})$ and integrate over the volume of grid cell Q. We obtain

$$\langle u_t + \nabla \cdot \mathbf{f}, \phi \rangle_Q = 0. \tag{4}$$

We proceed with an integration by parts

$$\langle u_t, \phi \rangle_Q + \langle \mathbf{f} \cdot \mathbf{n}, \phi \rangle_{\partial Q} - \langle \mathbf{f}^a - \mu \nabla u, \nabla \phi \rangle_Q = 0, \tag{5}$$

where $\mathbf{n}$ denotes the outward pointing normal vector and $\langle \dots \rangle_{\partial Q}$ the integral over the grid cell surface. As the approximative solution is in general discontinuous across grid cell interfaces, we need an approximation by numerical flux functions. For advection as well as diffusion we apply approximate Riemann solvers. While this is standard for advection, for diffusion it is described in [6] in detail. The semi-discrete version with discretization in space only we rewrite in a compact form as

$$\underline{\hat{u}}_t^Q = \mathscr{R}_V \left(\underline{\hat{u}}^Q, \underline{\varphi}^Q \right) + \mathscr{R}_S \left(\underline{\hat{u}}^Q, \underline{\hat{u}}^{Q^+}, \underline{\varphi}^Q \right), \tag{6}$$

where we collect all volume terms in $\mathscr{R}_V$ and all surface terms in $\mathscr{R}_S$. We indicate the dependence of the surface term on neighbor data by $\underline{\hat{u}}^{Q^+}$.

The set of ODE's (6) can now be integrated, where the time interval $[0;T]$ is subdivided into time levels t_n, by using for instance the standard Runge-Kutta methods, resulting in the classic Runge-Kutta discontinuous Galerkin method, see, e.g., [1].

In this paper a predictor corrector formulation is presented which picks up again the space-time nature of the equations . We start with an integration in time of the semi-discrete formulation (6) from time level t_n to time level t_{n+1}

$$\underline{\hat{u}}_{n+1}^Q - \underline{\hat{u}}_n^Q = \int_{t_n}^{t_{n+1}} \mathscr{R}_V \left(\underline{\hat{u}}^Q, \underline{\varphi}^Q \right) + \mathscr{R}_S \left(\underline{\hat{u}}^Q, \underline{\hat{u}}^{Q^+}, \underline{\varphi}^Q \right) dt. \tag{7}$$

The most efficient way to approximate the time integrals is to use Gauss quadrature. The problem is, that the DG solution is only known at the 'old' time level t_n. However, the Gauss points live in-between the time levels t_n and t_{n+1} and thus an implicit treatment or a predictor is needed for the evaluation of the volume and surface terms. A predictor is found by approximating the following *local Cauchy problems*: Find for every grid cell Q the function $v = v(\mathbf{x}, t)$ for $(\mathbf{x}, t) \in R^d \times [0; \Delta t]$, which satisfies the initial value problem

$$v_t + \nabla \cdot \mathbf{f}(v, \nabla v) = 0, \qquad v(\mathbf{x}, t = 0) = u^*(\mathbf{x}, t_n), \tag{8}$$

where $u^*(\mathbf{x},t_n)$ is the DG polynomial $u_Q(\mathbf{x},t_n)$ of grid cell Q extended in R^d. The idea is to solve this locally in every grid cell in a first step by any numerical method that produces a space-time solution of the desired order of accuracy.

2.1 The Predictor-Corrector Formulation

We propose in this paper to apply an explicit *local* Runge-Kutta Galerkin discretization to construct an approximative solution to the local Cauchy problems. Accordingly to the semi discrete DG scheme described above we introduce an approximation with the same polynomial degree

$$v_Q(\mathbf{x},t) = \sum_{j=1}^{N} \hat{v}_j^Q(t)\varphi_j^Q(\mathbf{x}) =: \underline{\hat{v}}^Q(t)\cdot\underline{\varphi}^Q(\mathbf{x}). \tag{9}$$

Inserting this into (8), multiplying by a test function and integrating over the grid cell Q yields the semi-discrete Galerkin formulation

$$\langle (v_Q)_t + \nabla\cdot\mathbf{f}(v_Q,\nabla v_Q),\phi\rangle_Q = 0, \tag{10}$$

and analogously the set of ODE's for the time dependent polynomial coefficients

$$\left(\underline{\hat{v}}^Q\right)_t = \mathscr{R}_V\left(\underline{\hat{v}}^Q,\underline{\varphi}^Q\right), \qquad \underline{\hat{v}}^Q(0) = \underline{\hat{u}}^Q(t_n). \tag{11}$$

We note that the local problem (8) does not involve DG data from neighbor grid cells. As stated above we aim to use a Runge-Kutta method to integrate (11) in time. However, to evaluate the space-time integrals in Eq. (7), a continuous approximation in time is needed. In [7, 8] a special Runge-Kutta based framework for the solution of such initial value problems was introduced, with the main feature that the approximation can be naturally extended to a time polynomial, hence the name *continuous extension Runge-Kutta (CERK) schemes*.

We observed, that for a desired time order $\mathscr{O}_t$ of the final scheme, we need one order less for the construction of the approximation of the local Cauchy problem $\mathscr{O}_t^* = \mathscr{O}_t - 1$. The evaluation of (7) with the approximation v_Q

$$\underline{\hat{u}}_{n+1}^Q - \underline{\hat{u}}_n^Q = \int_0^{\Delta t} \mathscr{R}_V\left(\underline{\hat{v}}^Q(t),\underline{\varphi}^Q\right) + \mathscr{R}_S\left(\underline{\hat{v}}^Q(t),\underline{\hat{v}}^{Q^+}(t),\underline{\varphi}^Q\right)dt, \tag{12}$$

increases the time order $\mathscr{O}_t$ by 1. Summing up, we have shown how to use a Runge-Kutta method to construct a time continuous local solution and insert this into the fully discrete DG scheme.

If we recall the semi-discrete Galerkin formulation of the local Cauchy problem (10), we notice that the volume integral is directly related to the time derivative of the auxiliary solution

$$\langle (v_Q)_t, \phi \rangle_Q = -\langle \nabla \cdot \mathbf{f}(v_Q, \nabla v_Q), \phi \rangle_Q, \qquad \text{or} \qquad \left(\underline{\hat{v}}^Q\right)_t = \mathscr{R}_V\left(\underline{\hat{v}}^Q, \underline{\varphi}^Q\right). \tag{13}$$

Inserting this into the volume term yields

$$\int_{t_n}^{t_{n+1}} \mathscr{R}_V\left(\underline{\hat{u}}^Q, \underline{\varphi}^Q\right) dt \approx \int_0^{\Delta t} \mathscr{R}_V\left(\underline{\hat{v}}^Q, \underline{\varphi}^Q\right) dt = \int_0^{\Delta t} \underline{\hat{v}}_t^Q \, dt = \underline{\hat{v}}^Q(\Delta t) - \underline{\hat{v}}^Q(0). \tag{14}$$

Due to the construction of the auxiliary solution we have $\underline{\hat{v}}^Q(0) = \underline{\hat{u}}_n^Q$.

The strong variant of the fully discrete DG scheme (12) yields the *predictor-corrector formulation*

$$\underline{\hat{u}}_{n+1}^Q = \underline{\hat{v}}^Q(\Delta t) + \int_0^{\Delta t} \mathscr{R}_S\left(\underline{\hat{v}}^Q(t), \underline{\hat{v}}^{Q^+}(t), \underline{\varphi}\right) dt. \tag{15}$$

This formulation shows, that the DG solution at the new time level $\underline{\hat{u}}^{n+1}$ is determined by the value of the prediction at the new time level $\underline{\hat{v}}^Q(\Delta t)$ (note that the predictor does not take any neighbor data into account) corrected with the surface integral term, where information from the local and the neighbor grid cells is taken into account.

3 Local Time-stepping

The most important property of this predictor-corrector formulation is its inherent locality valid for the whole time step. The disadvantage of an explicit time approximation, to advance with the smallest time step determined by all local stability restrictions, can be dropped by a time accurate local time stepping. The time evolution is shown in Fig.3. A grid cell Q_i is evolved from t_i^n to $t_i^{n+1} = t_i^n + \Delta t_i$ under the condition that the predictor (light gray) of the neighbor cells Q_j is available $t_i^{n+1} \leq t_j^{n+1}$. This evolve condition guarantees the time-consistency needed for unsteady problems. In Fig.3a, all predictors are calculated and Q_2 fulfills the evolve condition. In Fig.3b, the corrector, consisting of the surface integrals, is then applied to Q_2, a new predictor can be computed and now Q_3 can evolve. The algorithm continues analogously, see Fig.3c-d. If we take a careful look at the corrector, the spatial integral can be approximated with Gauss integration, yielding to the general form

$$\int_{t_i^n}^{t_i^{n+1}} \oint_{\partial Q_i} h(\mathbf{x},t)\varphi_j(\mathbf{x})\, ds\, dt = \int_{t_i^n}^{t_i^{n+1}} \sum_{k=1}^{M} \tilde{h}_k(t)\, \omega_k^j \; dt = \sum_{k=1}^{M} \left(\int_{t_i^n}^{t_i^{n+1}} \tilde{h}_k(t)\, dt \right) \omega_k^j = \sum_{k=1}^{M} H_k\, \omega_k^j, \tag{16}$$

where $h(\mathbf{x},t)$ is the numerical flux, depending on the local and neighbor predictor, $\tilde{h}_k(t) = h(\xi_k, t)$ its value at the spatial point. The weights ω_k^j contain the evaluation

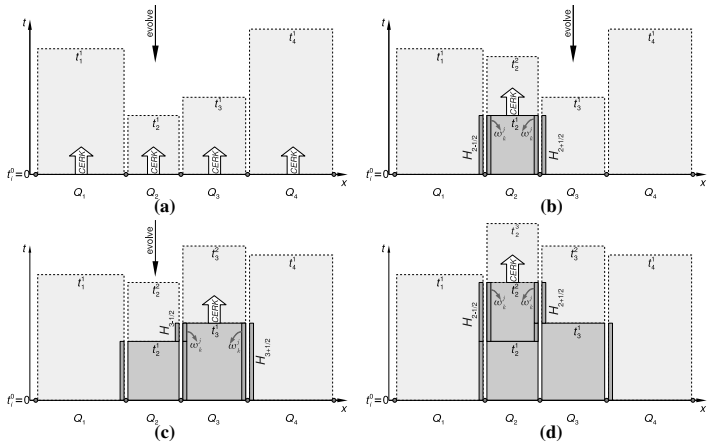

Fig. 1 Time evolution of the local time stepping algorithm in 1D with 4 grid cells

of $\varphi_j(\xi_k)$ and are calculated once at the beginning of the calculation, since they are time-independent. Furthermore, integration and summation can be changed. Now only the *time integrated flux* $H_k = H(\xi_k, [t_i^n, t_i^{n+1}])$ at evaluation point ξ_k remains to be calculated. We will first integrate the fluxes in time and then in space. The remedy can be seen in Fig.3c at the interface Q_2, Q_3. The time integrated flux $[t_2^0, t_2^1]$ is temporarily saved. We only add $H(\xi_k, [t_2^1, t_3^1])$, before applying the final space integration. This is crucial for the efficiency of the local time-stepping algorithm.

References

1. B. Cockburn and C.-W. Shu. The Runge-Kutta discontinuous Galerkin method for conservation laws V: Multidimensional systems. *J. Comput. Phys.*, 141:199–224, 1998.
2. M. Dumbser, D. S. Balsara, E. F. Toro, and C.-D. Munz. A unified framework for the construction of one-step finite-volume and discontinuous Galerkin schemes on unstructured meshes. *J. Comput. Phys*, 227:8209–8253, 2008.
3. M. Dumbser, C. Enaux, and E. F. Toro. Finite volume schemes of very high order of accuracy for stiff hyperbolic balance laws. *J. Comput. Phys.*, 227:3971–4001, 2008.
4. A. Harten, B. Engquist, S. Osher, and S. R. Chakravarthy. Uniformly high order accurate essentially non-oscillatory schemes, iii. *Journal of Computational Physics*, 71(2):231 – 303, 1987.
5. F. Lörcher, G. Gassner, and C.-D. Munz. A discontinuous Galerkin scheme based on a space-time expansion. I. Inviscid compressible flow in one space dimension. *J. Sci. Comp.*, 32(2):175–199, 2007.
6. F. Lörcher, G. Gassner, and C.-D. Munz. An explicit discontinuous Galerkin scheme with local time-stepping for general unsteady diffusion equations. *J. Comput. Phys.*, 227(11):5649–5670, 2008.
7. B. Owren and M. Zennaro. Order barriers for continuous explicit Runge-Kutta methods. *Math. Comp.*, 56:645–661, 1991.
8. B. Owren and M. Zennaro. Derivation of efficient continuous explicit Runge-Kutta methods. *SIAM J. Sci. Stat. Comput.*, 13:1488–1501, 1992.

Multi-dimensional Limiting Process for Discontinuous Galerkin Methods on Unstructured Grids

Jin Seok Park and Chongam Kim

Abstract The present paper deals with the continuous work of extending the multi-dimensional limiting process (MLP), which has been quite successful in finite volume methods (FVM), into discontinuous Galerkin (DG) methods. Based on successful analyses and implementations of the MLP slope limiting in FVM, MLP is applicable into DG framework with the MLP-based troubled-cell marker and the MLP slope limiter. Through several test cases, it is observed that the newly developed MLP combined with DG methods provides quite desirable performances in controlling numerical oscillations as well as capturing key flow features.

1 Introduction

Multi-dimensional limiting process (MLP) has been developed quite successfully in finite volume methods (FVM). Compared with traditional limiting strategies, such as TVD or ENO-type schemes, MLP effectively controls unwanted oscillations particularly in multiple dimensions. The theoretical foundation of the MLP limiting strategy is to satisfy the maximum principle to ensure multi-dimensional monotonicity. A series of researches [2, 6, 4] clearly demonstrates that the MLP limiting strategy possesses superior characteristics in terms of accuracy, robustness and efficiency in inviscid and viscous computations on structured and unstructured grids in FVM. Recently, discontinuous Galerkin (DG) methods become more popular as a higher-order discretization of hyperbolic conservation laws because of its own mer-

Jin Seok Park
School of Mechanical and Aerospace Engineering, Seoul National University, Seoul 151-744, Korea, e-mail: seok82@snu.ac.kr

Chongam Kim
Institute of Advanced Aerospace Technology, School of Mechanical and Aerospace Engineering, Seoul National University, Seoul 151-744, Korea, e-mail: chongam@snu.ac.kr, Corresponding author

its, such as flexibility to handle complex geometry, compact stencil for higher-order reconstruction, and amenability to parallelization and hp-refinement. However, one of the major bottlenecks in DG methods is to design a robust, accurate and efficient limiting strategy to handle oscillations and discontinuities in multiple dimensions. Although there have been several remarkable efforts to control oscillations using TVB-based limiters or WENO-type limiters, overall performances are not satisfactory at all in terms of accuracy and/or efficiency, especially in controlling oscillations near shock discontinuities in multi-dimensional flows. Based on the remarkable successes of the MLP in FVM, the MLP limiting philosophy is now extended into the DG framework to provide an accurate, efficient and robust limiting strategy.

2 Multi-dimensional Limiting Process

2.1 Multi-dimensional Limiting Condition

In order to maintain multi-dimensional monotonicity, the present limiting strategy exploits the MLP condition, which is an extension of the one-dimensional monotonic condition. The basic idea of the MLP condition is to control the distribution of both cell-centered and cell-vertex physical properties to mimic a multi-dimensional nature of flow physics. We focus on the observation that well-controlled vertex values at interpolation stage make it possible to produce monotonic distribution of cell-averaged values. This observation is verified by showing that cell-centered and cell-vertex values reconstructed by the MLP limiting safisfy the maximum principle. Based on the observation, the vertex values are required to satisfy the following MLP condition

$$\bar{q}^{min}_{neighbor} \leq q_{vtx} \leq \bar{q}^{max}_{neighbor}, \tag{1}$$

where q_{vtx} is the vertex value, and $(\bar{q}^{min}_{neighbor}, \bar{q}^{max}_{neighbor})$ are the minimum and maximum cell-averaged values sharing the same vertex point. The MLP condition can be implemented regardless of grid topology, though the present work is focused on triangular mesh. For example, the detailed implementation in FVM can be seen in the work of Ref. [2, 6] for structured grids and Ref. [4] for unstructured grids. The effectiveness of the MLP condition is supported by the maximum principle, which plays a key role in ensuring the monotonicity in multiple dimensions. Compared to previous approaches, the MLP condition fully exploits the cell-averaged values sharing the same vertex point as well as edges, so the MLP limiting is less sensitive to local mesh distribution and accurately represents multi-dimensional flow physics.

3 Extension of MLP into Discontinuous Galerkin Methods

In DG methods, the distribution within a cell is approximated by the sum of shape modes in a suitable function space

$$q_j^h(\mathbf{x},t) = \sum_{i=1}^{n} q_j^{(i)}(t) b^{(i)}(\mathbf{x}), \tag{2}$$

where q_j^h is an approximated solution of $q(\mathbf{x},t)$ on the cell T_j and $b^{(i)}$ is a shape function. In the present work, the RKDG method with orthogonal shape functions is adopted. In order to prevent unwanted oscillations near discontinuities, limiting procedure is essential. Especially for efficient and accurate computations, limiter should be selectively activated on the troubled-cells only. Thus, an accurate troubled-cell marker, as well as a limiter, is crucial to obtain an accurate monotone solution in the DG framework.

In FVM, the MLP condition is used to identify and control the maximum-principle-violating cells [4]. If property distribution is linear, the edge midpoint (or any quadrature point) can be restricted by controlling the vertex points where extrema occur. However, for higher-order reconstruction greater than P1, it is not guaranteed. The P1-based MLP condition may not identify the troubled-cells which may lead to violation of the maximum principle. After some analysis, a more strict condition is found to be necessary to identify the troubled cells. The MLP-based troubled-cell marker is proposed using the following augmented MLP condition

$$\bar{q}_{v_i}^{\min} \le q_{v_i}^{h,\min} \le q_{v_i}^h, \;\; q_{v_i}^h \le q_{v_i}^{h,\max} \le \bar{q}_{v_i}^{\max}, \tag{3}$$

where $q_{v_i}^h$ is an approximated solution at vertex v_i and $(\bar{q}_{v_i}^{\min}, \bar{q}_{v_i}^{\max})$ are minimum and maximum among the cells sharing the vertex. If distribution at vertex violates the above condition, this cell is marked as a troubled cell. To avoid the clipping problem across local smooth extrema, a simple but effective extrema detector is additionally introduced as follows

$$\Delta \bar{q}_{v_i} = \bar{q}_{v_i}^{\max} - \bar{q}_{v_i}^{\min} \le K \Delta x^2, \tag{4}$$

where K is a parameter to be determined. Numerical experiments strongly indicate that computed results are not sensitive to the change of K, and its optimal value is around 100. With the augmented MLP condition (Eq. (3)) and the extrema detector (Eq. (4)), the troubled-cells are marked and the MLP slope limiter is applied only on these cells with the following distribution

$$\tilde{q}_j^h(\mathbf{x},t) = \bar{q}_j + \phi_{MLP} \nabla q_j \cdot (\mathbf{x} - \bar{\mathbf{x}}_\mathbf{j}). \tag{5}$$

For the Euler systems, density or entropy variable is used in the troubled-cell marker to identify physical discontinuities. After marking the troubled-cells, the MLP limiting is applied on conservative variables, the same as in the MLP in FVM.

4 Numerical Result

4.1 Compressible Flow with Sinusoidal Density Perturbation

In order to examine accuracy in continuous flow, the Euler system with the following smooth initial data is considered

$$(\rho_0, u_0, v_0, p_0) = (1 + 0.2sin(\pi(x+y)), 0.7, 0.3, 1.0). \tag{6}$$

The computational domain is $[0,2] \times [0,2]$ with periodic boundary condition. Triangular elements are created by dividing uniform square elements along the diagonal. Table 1 shows the result of grid refinement test at $t = 2$. The MLP limiting combined with the MLP troubled-cell marker ($K = 100$) preserves the designed accuracy in DG reconstruction.

Table 1 Grid refinement test for compressible flow with sinusoidal density perturbation

	DG-P1, MLP-u1, K=100				DG-P2, MLP-u1, K=100			
Grid	L_∞	Order	L_1	Order	L_∞	Order	L_1	Order
10x10x2	1.774E-2	-	1.046E-2	-	8.137E-4	-	4.279E-4	-
20x20x2	3.411E-3	2.38	1.919E-3	2.45	1.046E-4	2.96	5.242E-5	3.03
40x40x2	7.019E-4	2.28	3.743E-4	2.36	1.326E-5	2.98	6.527E-6	3.01
80x80x2	1.543E-4	2.18	7.965E-5	2.23	1.664E-6	2.99	8.159E-7	3.00

4.2 A Mach 3 Wind tunnel with a Step

This is one of the popular cases to test higher-order high-resolution schemes. Around the expansion corner, computational meshes are slightly clustered without any special treatment. Lax-Friedrich scheme is applied as a numerical flux. Figure 1 shows the density contours computed on triangular grids of $h = 1/160$ at $t = 4.0$. DG reconstructions with the MLP limiter provide monotonic solutions with a sharp capturing of the slip line from the shock triple point.

4.3 Strong Vortex-Strong Shock Interaction

Shock-vortex interaction generally leads to complex but challenging flow patterns. When the rapidly rotating vortex strikes the strong shock, vortex core is severely elongated and eventually split by compression [5]. The computational domain is $[0,2] \times [0,1]$ and the normal shock wave with $M_s = 1.5$ is located at $x = 0.5$. A

composite vortex is located at $(x_c, y_c) = (0.25, 0.5)$, and the velocity profile is given as follows

$$v_\theta = \begin{cases} v_m \frac{r}{a} & \text{if } r \le a \\ v_m \frac{a}{a^2-b^2}\left(r - \frac{b^2}{r}\right) & \text{if } a \le r \le b \\ 0 & \text{if } r > b \end{cases}, \tag{7}$$

where $(a, b) = (0.075, 0.175)$, and the maximum Mach number of angular velocity is 0.9. AUSMPW+ scheme [1] is used as a numerical flux. In Fig. 2, numerical Schlieren images computed by FVM and DG reconstructions with the MLP limiter are compared at $t = 0.7$ on coarse and fine grids. While FVM-MLP on coarse grid does not show the vortex-splitting phenomenon, DG P2-MLP captures this flow structure very clearly. In addition, DG reconstruction with the MLP limiter provides a more detailed resolution for emitted sound waves and discontinuities.

4.4 Interaction of Shock wave with 2-D Wedge

The computational domain contains a regular triangle with length $L = 1$ on $[-2.5, 4.6] \times [-2.5, 2.5]$. The tip of wedge is located at the origin. As an initial condition, the moving shock with $Ms = 1.34$ is located at $x = 0$. RoeM flux scheme [3] is applied. Figure 3 shows the comparison of numerical Schlieren images at $t = 3.25$. Computed results confirm again that the DG reconstruction with the MLP limiter guarantees a sufficient resolution to capture complex shock-vortex structure.

5 Conclusion

Guided by the MLP condition and the maximum principle [4], the Multi-dimensional limiting process is efficiently and accurately designed within discontinuous Galerkin framework. The proposed approach is able to accurately capture complex multi-dimensional flow structure without yielding unwanted oscillations. Various numerical results show the desirable characteristics of the proposed limiting strategy, such as multi-dimensional monotonicity, improved accuracy and efficiency.

Fig. 1 Comparison of density contours for the Mach 3 wind tunnel with a step. Thirty equally spaced contour lines from $\rho = 0.32$ to $\rho = 6.15$

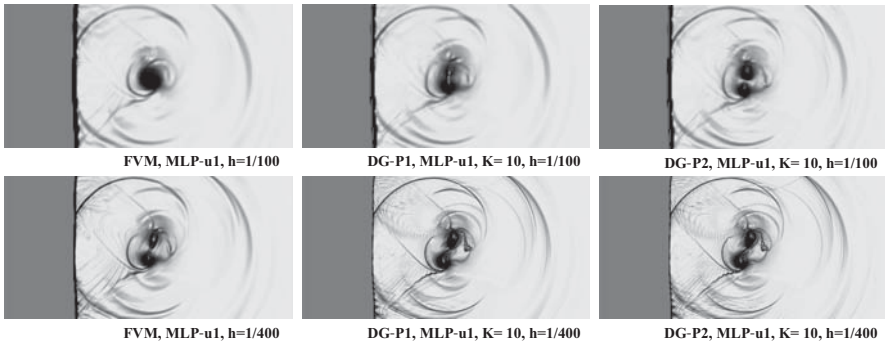

Fig. 2 Comparison of numerical Schlieren images of strong vortex-strong shock problem at $t = 0.7$

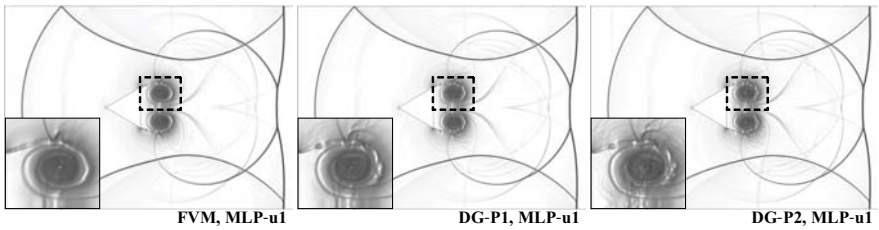

Fig. 3 Comparison of numerical Schlieren images on interaction of shock wave with 2-D wedge at $t = 3.25$. (Bottom left corner of each image: Close-up view around the primary vortex.)

Acknowledgements Authors appreciate the financial supports provided by NSL (National Space Lab.) program through the National Research Foundation of Korea funded by the Ministry of Education, Science and Technology (Grant 20090091724), and by National Institute for Mathematical Sciences.

References

1. Kim, K.H., Kim, C., Rho,O.H.: Methods for the accurate computations of hypersonic flows, part I: AUSMPW+ scheme, J. Comput. Phys. **174** 38-80. (2001)
2. Kim, K.H., Kim, C.:Accurate, efficient and monotonic numerical methods for multi-dimensional compressible flows: Part II: Multi-dimensional limiting process. J. Comput. Phy. **208**, 570-615 (2005)
3. Kim, S., Kim, C., Rho, O. H., Hong S. K.: Cures for the shock instability: Development of a shock-stable Roe scheme, J. Comput. Phys. **185** 342-374. (2003)
4. Park, J.S., Yoon, S-.H., Kim, C.: Multi-dimensional limiting process for hyperbolic conservation laws on unstructured grids. J. Comput. Phy. **229**, 788-812 (2010)
5. Rault, A., Chiavassa, G., Donat, R.: Shock-vortex interactions at high Mach numbers, J. Sci. Comput. **19** 347-371 (2003)
6. Yoon, S-.H., Kim, C., Kim, K.H.: Multi-dimensional limiting process for three-dimensional flow physics analyses. J. Comput. Phy. **227**, 6001-6043 (2008)

Runge Kutta Discontinuous Galerkin to solve reactive flows

Germain Billet & Juliette Ryan

1 Introduction

Phenomena which develop in the combustion chambers or industrial furnaces are multiple. Injections of fuel and oxidizer, premixed or not, in a strongly turbulent flow set up gas pockets which react generating either premixed flames or diffusion flames together with intense acoustic phenomena. These physical processes have to be captured in order to describe in details the reactive flows. It is then necessary to take into account the transport coefficients for the parabolic operator of the Navier-Stokes (*NS*) equations and detailed chemical kinetics for the production rates (source operator). Vortex dynamics, transport, stretching and wrinkling of fronts as well as acoustic propagation must be suitably resolved by the hyperbolic operator.

Within the framework of the Euler equations, we found two recent articles [8] , [11] which propose to solve the two-medium flow simulations starting from a Runge-Kutta Discontinuous Galerkin (*RKDG*) method. Both use the level set method to compute the location of the interface. The advantage is to keep a conservative treatment of the interface but the difficulty lies in the coupling between a traditional *RKDG* method far from the interface and a Discontinuous Galerkin (*DG*) level set method around the interface. The level set method is very powerful and is used in many fields but its main weakness is that it can only treat nondiffusive interfaces. Its use in the field of the reactive flows is thus limited to the follow-up of thin front with very reductive assumptions as to the reactive processes. For the reacting porous media, some approaches using *DG* to solve reacting *NS* equations have been developed but generally the incompressibility hypothesis is introduced, see for example [12]. In addition, many papers have presented the resolution of *NS* equations with *RKDG* method for nonreactive flows with a constant specific heat ratio γ. But when the fluid contains Ns gaseous species in a flow where the temperature T evolves strongly as in reactive flows, it is necessary to take into account

Germain Billet, e-mail: billet@onera.fr, Juliette Ryan, e-mail: ryan@onera.fr
ONERA, BP72 - 29 avenue de la Division Leclerc, FR-92322, CHATILLON CEDEX, FRANCE,

the variation of γ and to assume $\gamma = \gamma(Y_i, T)$ where Y_i is the mass fraction of the ith species ($i \in \mathscr{S} = [1, Ns]$). In the same way, the transport coefficients depend on the same variables.

We describe here a *RKDG* method with no restrictive physical hypothesis to solve the reactive Navier-Stokes equations written in conservation form. For the time integration, a third-order *TVD* Runge-Kutta scheme is used [10]. One test case is presented with DGP^1 and DGP^2 which simulates 2-D premixed flames H_2-air with a simplified kinetic scheme.

2 The Discontinuous Galerkin approach

This approach is based on the work of Cockburn and Shu (see [4]). For simplicity, we shall just recall the 1D case, representative of all dimensions. The solution as well as the test function space is given by

$\mathscr{W}_h^k = \left\{ \varphi \in L^\infty(\Omega) \ / \ \forall j, \varphi_{|\Omega_j} \in P^k(\Omega_j) \right\}$ where $P^k(\Omega_j)$ is the space of polynomials of degree $\leq k$ on the cell $\Omega_j = [x_{j-1/2}, x_{j+1/2}] = \Delta x_j$. We define a local orthogonal basis over Ω_j, $\{\phi_j^{(l)}(x), l = 0, 1, ..., k\}$ where $\phi_j^{(l)}(x)$ are the Legendre polynomials. The numerical solution in the test function space $\mathscr{W}_h^k$ is written as

$$\forall t \in [0,T], \forall x \in \Omega_j, \ \mathscr{U}^h(x,t) = \sum_{l=0}^{l=k} \mathscr{U}_j^{(l)}(t) \phi_j^{(l)}(x) \text{ for } x \in \Omega_j$$

where $\mathscr{U}_j^{(l)}(t)$ are the degrees of freedom. A weak formulation of the problem is obtained by multiplying the *NS* equations by a test function φ and by integrating on each cell Ω_j. Then, a discrete analogous is obtained by replacing the exact solution $\mathscr{U}$ by the approximation $\mathscr{U}^h(x,t)$, $\forall t \in [0,T], \forall j$,

$$\int_{\Omega_j} \varphi(x) \frac{\partial \mathscr{U}^h(x,t)}{\partial t} dx + \int_{\Omega_j} \varphi(x) \frac{\partial \mathscr{F}(\mathscr{U}^h(x,t))}{\partial x} dx = \int_{\Omega_j} \varphi(x) \mathscr{S}(\mathscr{U}^h(x,t)) dx.$$

The test function φ is replaced by each element of the basis set $\phi_j^{(l)}(x)$ and the inviscid and viscous fluxes are integrated by part. The source term $\mathscr{S}$ represents the production rates of each species.

3 Hyperbolic operator

The main difficulty is to capture correctly the gaseous interfaces. If no care is taken to solve the hyperbolic part of the Navier-Stokes equations in conservative form, spurious pressure oscillations develop when several species diffuse through an in-

terface where γ varies [6], [1]. Some models were proposed in the past but, either they present other disadvantages like the appearance of oscillations on other quantities, or they are written for particular cases of front capturing or for mixtures where C_P is supposed constant. In 2001, Abgrall and Karni [2] proposed the DF model for mixtures where C_P depends only on the mass fractions. In 2003, Billet and Abgrall [3] generalized this approach for $C_P = C_P(Y_i, T)$. This approach, which is no longer strictly conservative but only quasi-conservative for the hyperbolic part of NS equations when γ varies, suppresses the numerical oscillations of the physical quantities through the gas interfaces. DF is efficient only with numerical fluxes which can be extended to a complex thermodynamic laws $\gamma = \gamma(Y_i, T)$ as for example $HLLC$ [13]. A limiting treatment based on Krivodonova's paper [5] is applied for DGP^2 when the reactive processes are activated.

4 Parabolic operator

The recovery method reproduces the symmetric DG formulation with natural penalty terms depending on the accuracy of the method. Van Leer's idea is to construct for each piecewise continuous polynomial basis of degree k defined on two adjacent cells a unique continuous polynomial space of degree $2k+1$ on the union of the two cells. In consequence, to the approximation of the solution as an expansion in the discontinuous basis functions locally corresponds an identical expansion in the smooth recovery basis. Thanks to this new smooth basis, the diffusion fluxes across the cell interfaces can be naturally computed. The details of this approach can be found in [15] for the 1-D problems and the extension to 2-D is developed in [14]. In reactive flows, the transport coefficients are not uniform and consequently the diffusive part of the NS equations are integrated by part once only.

5 Numerical example

5.1 Draughtboard reactive mixing H_2-Air in a shear flow

We are interested in a draughtboard mixture of H_2-Air (simulating the region of an idealized multi-point injector). This mixture is immersed in a sinusoidal temperature field varying between $300K$ and $1200K$. This gaseous mixing is also submitted to in a sinusoidal velocity field varying for each component u and v between $-100m/s$ and $+100m/s$. With these values, the Mach number M varies in the range $-0.4 < M < 0.4$ during the computation. Four shear lines are present in the flow at $t = 0$ ($x = 0m$, $x = 0.05m$, $y = 0.025m$ and $y = 0.075m$). The domain dimensions are $L^2 = 0.1m$ x $0.1m$ and the boundary conditions are periodic. A Cartesian grid is used with $\Delta x = \Delta y$. The mixture wave length $L_\lambda^Y = L/4$ and the wave length of temperature

and velocity fields are $L_\lambda^T = L_\lambda^u = L_\lambda^v = L$. At $t = 0$,

$$\begin{aligned}
T &= 750 - 450\sin(2\pi x/L_\lambda^T)\sin(2\pi y/L_\lambda^T)\\
u &= -100\sin(2\pi x/L_\lambda^u)\cos(2\pi y/L_\lambda^u)\\
v &= -100\sin(2\pi x/L_\lambda^v)\cos(2\pi y/L_\lambda^v)\\
Y_{O_2} &= 0.117(1+\sin(2\pi x/L_\lambda^Y)\sin(2\pi y/L_\lambda^Y))\\
Y_{H_2} &= 0.015(1-\sin(2\pi x/L_\lambda^Y)\sin(2\pi y/L_\lambda^Y))\\
Y_{N_2} &= 1 - Y_{O_2} - Y_{H_2}.
\end{aligned}$$

Some initial fields are plotted in Fig.1. The time step $\delta t = 5\times 10^{-8}s$ corresponds to $Cfl = 0.1$. The kinetic scheme is made up of 4 species and 2 Arrhenius reactions [9]:

$$H_2 + O_2 \leftrightarrow 2OH \;\text{ and }\; H_2 + 2OH \leftrightarrow 2H_2O.$$

Figs. 2 and 3 present the time evolution of the temperature with DGP^1 and DGP^2 on a same grid ($L_\lambda^Y = 8\Delta x$). At $t = 10^{-3}s$, the solutions are similar but more details appear with DGP^2. But at $t = 2\times 10^{-3}s$, the topology of the temperature field is quite different and the temperature levels are no longer the same. These differences are due to the very strong acoustic waves that develop at the beginning of the reactions. DGP^2, thanks to its weaker dissipation, captures better these strong fluctuations and gives after $t = 10^{-3}s$ a different shape of the flames in the domain.

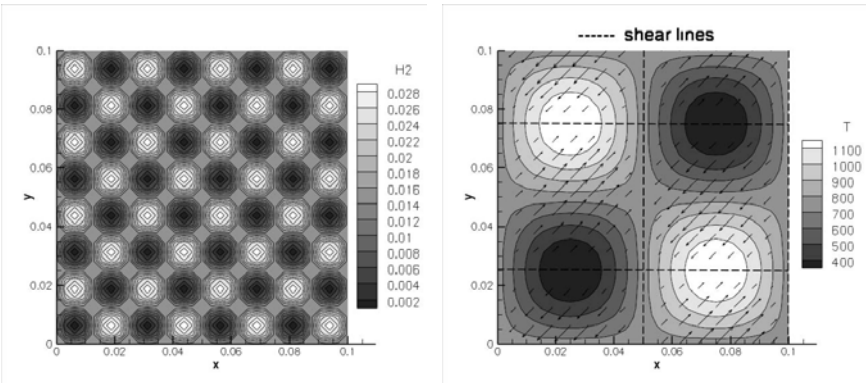

(a) Initial hydrogen mass fraction. (b) Initial velocity and temperature fields (K).

Fig. 1 Initial values.

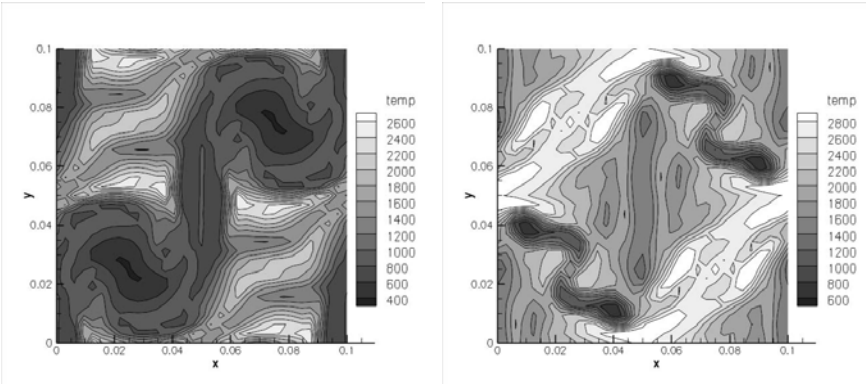

(a) Temperature field at t=10^{-3} s. (b) Temperature field at t=2×10^{-3} s.

Fig. 2 Temperature fields with DGP^1.

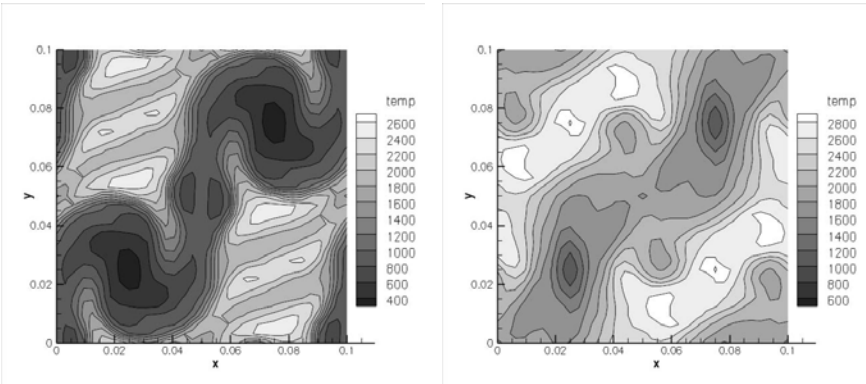

(a) Temperature field at t=10^{-3} s. (b) Temperature field at t=2×10^{-3} s.

Fig. 3 Temperature fields with DGP^2.

6 Conclusion

A *RKDG* approach with no restrictive physical hypothesis has been developed for reactive flows. This approach is stable and robust and works well for low Mach number and subsonic flows. Its extension to supersonic combustion is under development. Comparisons with a sixth order finite difference DNS code with detailed kinetic scheme [7] are to be carried out.

References

1. R. Abgrall: How to prevent pressure oscillations in multicomponent flows: a quasi conservative approach. *J. Comput. Phys*. 125, (1996).
2. R. Abgrall , S. Karni: Compressible multifluids. *J. Comput. Phys.*, 169, (2001).
3. G. Billet, R. Abgrall: An adaptive shock-capturing algorithm for solving unsteady reactive flows. *Comput. & Fluids,* 32, (2003).
4. B. Cockburn, C-W. Shu: The Runge-Kutta Discontinuous Galerkin method for conservation laws V: multidimensional systems. *J. Comput. Phys*. 141, (1998).
5. L. Krivodonova: Limiters for high-order discontinuous Galerkin methods. *J. Comp. Phys.* 226 (2007).
6. B. Larouturou: How to preserve the mass fraction positive when computing compressible multicomponent flows. *J. Comput. Phys*. 95, (1991).
7. A. Laverdant, D. Thevenin: Interaction of a gaussian acoustic wave with a turbulent premixed flame. *Comb. & Flame.* 134, (2003).
8. J. Qiu, T. Liu and B. C. Khoo: Runge-Kutta Discontinuous Galerkin methods for compressible two-medium flows simulations: one-dimensional case; *J. Comput. Phys*. 222, (2007).
9. R. C. Rogers & W. Chinitz: Using a global hydrogen-air combustion model in turbulent reacting flow calculations. *AIAA journal,* Vol.21, n4, (1983).
10. C-W. Shu, S. Osher: Efficient implementation of, essentially non-oscillatory shock-capturing schemes. *J. Comput. Phys.* 77, (1998).
11. W.E.H. Sollie, J.J.W. van der Vegt & O. Bokhove: A space-time discontinuous galerkin finite element method for two-fluid problems. *memorandum 1849, University of Twente*, (2007).
12. S. Sun & M.F. Wheeler: Analysis of Discontinuous Galerkin for multicomponent reactive transport problems. *Comp. & Math. Applic*., (2006).
13. E.F. Toro, M. Spruce & W. Spears: Restoration of the contact surface in the HLL riemann solver. *Shock waves* 4, (1994).
14. B. van Leer, M. Lo, M. van Raalte: A discontinuous Galerkin method for diffusion based on recovery. *18th AIAA CFD conference*, (2007).
15. M. van Raalte, B. van Leer: Bilinear forms for the recovery-based discontinuous Galerkin method for diffusion. *Proceedings ICFD 2007*, (2007).

Comparison of the high-order compact difference and discontinuous Galerkin methods in computations of the incompressible flow

Artur Tyliszczak, Maciej Marek and Andrzej Boguslawski

Abstract High-order compact difference scheme (CD) based on the half-staggered mesh is compared with discontinuous Galerkin method in computations of the incompressible flow. Assessment of the accuracy is performed based on the classical test cases: Taylor-Green vortices, Burggraf flow and also for temporally evolving shear layer. The CD method method provides very accurate results with expected order of accuracy, 4th and 6th. Similarly for the discontinuous Galerkin method provided that the number of degrees of fredom is close to the number of nodes in computations with CD method. Furthermore, it appeared that CD method is much more efficient than the discontinuous Galerkin method of comparable accuracy.

1 Introduction

The most accurate spectral or pseudospectral methods [1] based on Fourier or Chebyshev approximation allow for detailed study of complex fundamental physical phenomena. Their application is however limited to simple geometries and meshes defined by the collocation points which means that in geometrically complicated problems they are no longer feasible. The coordinate transformation combined with the domain decomposition are not always possible but even if so, this approach considerably complicates the numerical codes and sometimes leads to additional problems related to stability, singularity, etc.. The compact difference schemes [6] can be regarded as an alternative of the spectral approach sharing their most important properties (accuracy, resolving efficiency). Additionally, they can be easier applied in the cases of non-uniform and non-cartesian grids with various type of the boundary conditions. The finite volume, the finite element or discontinuous Galerkin approach are examples of the methods without any particular geometrical or mesh

Artur Tyliszczak, Maciej Marek and Andrzej Boguslawski
Czestochowa University of Technology, Al. Armii Krajowej 21, 42-200 Czestochowa, Poland.
e-mail: {atyl, marekm, abogus}@imc.pcz.czest.pl

related limitations. In this work we compare two of the above mentioned methods, the compact difference method and the discontinuous Galerkin method applied to the incompressible flow calculations.

2 Numerical methods

Both for the discontinuous Galerkin method and for the compact difference method we apply the projection method [3] which after the pressure correction step enforces the divergence free velocity field. In the compact difference (CD) approach we use half-staggered meshes [5, 10] where the pressure is shifted half cell size with respect to the velocity field. This approach eliminates the pressure oscillation caused by the pressure-velocity decoupling occurring on the collocated meshes. In the half-staggered approach additional computational cost and complications are related to the mid-point interpolation and mid-point derivative approximation, however we note that these steps are less computationally expensive than in the case of the fully staggered approach. We also note that shifting the pressure half-cell size from the velocity node is relatively easy and can be surely applied to any code based on the collocated meshes - that was done in our case. Another important point concerns solution of the Poisson equation (introduced by the projection method) which in the case of the high-order methods can be very expensive computationally as the resulting coefficient matrix of the Poisson equation is dense. Solving the Poisson equation we combine a low-order pressure gradient discretization with an explicit high-order discretization of the divergence operator. The resulting discretization has similar resolving characteristics as the compact scheme but it leads to 5 or 7-diagonal system which can be effectively solved by a direct method for sparse systems (analogy of TDMA algorithm).

The discontinuous Galerkin method (DGM) belongs to the family of finite element methods (FEM) and allows for employment of unstructured flexible computational meshes. Moreover, *hp*-adaptivity is much easier to implement, comparing to classical continuous Galerkin method, as the method supports non-conforming elements (hanging nodes) and possibility of various expansion bases (shape functions). The locality of DGM makes it an ideal framework for parallelisation. The matrices, that are typically constructed in FEM (e.g. mass matrix), can be calculated seperately for each element and their size is related to the number of local degrees of freedom. DGM has also some drawbacks, the main being larger number of variables comparing to continuous Galerkin method and additionally the second order derivatives (e.g. viscosity, diffusion terms, Laplacian) have to be handled by mixed methods. In the present work the implementation of DGM method has been developed for 2D incompressible, viscous flow. The code accepts unstructured FEM meshes with quadrilateral elements. Such meshes offer better quality, comparing to those with triangular elements. Also the basis functions may be constructed in a straightforward way by tensor products of one-dimensional functions [2, 4, 8]. The disadvantage is that the Jacobian of transformation from the standard element to the

physical element is not constant (in general), which results in considerable storage requirements – DGM matrices must be constructed for each of the elements seperately. The second order terms, representing viscosity and Laplacian of the pressure, are handled by LDG (Local Discontinuous Galerkin) method. The solver of Poisson equation for the pressure is based on simple, iterative method.

3 Results

The comparison of the accuracy and efficiency of the compact and discontinuous Galerkin methods is performed for classical test cases, i.e. Taylor-Green vortices, Burggraf flow and also for temporal shear layer flow. Both codes were written in the Fortran 90 with mathematical libraries (Lapack/BLAS) used wherever possible. The test of the efficiency showed that the code based on CD scheme is considerably faster than the code based on DG method. For instance, for the CD scheme, the computations of the Taylor-Green flow (simulation time equal to 1.0 with $\Delta t = 10^{-5}$) on the mesh 100×100 took about 45 minutes. For the DG method the accuracy of the results similar to that obtained with CD was achieved with 20×20 elements with 4th order of expansion, in this case the computations took 10 hours, approximately.

3.1 Taylor-Green and Burggraf flows

The Taylor-Green or Burggraf flow are examples of the test cases for which the analytical solution of the Navier-Stokes equations exists and therefore these cases are used in this work to assess the order of the applied methods. Fig. 1 shows parts of the computational domains with contours of the horizontal velocity component obtained with 6th order compact difference method with 3th and 4th order approximation for the near boundary and boundary nodes. Fig. 1 on the right hand side presents the error decreasing with the number of mesh points N. The error is defined as:

$$Error = \sqrt{\frac{1}{N_x}\frac{1}{N_y}\sum_{i=1}^{N_x}\sum_{i=1}^{N_y}\left(u_c(x_i,y_j) - u_a(x_i,y_j)\right)^2} \tag{1}$$

where u_c and u_a are computed and analytical value respectively. We note that in the computations performed with CD scheme for the velocity components we applied Dirichlet boundary conditions resulting from the analytical solution - typically (and also in our implementation of the discontinous Galerkin method) the Taylor flow is solved with the periodic boundaries which eliminate the influence of the lower order boundary closure scheme. Besides that, as the number of the boundary nodes is small compared to all computational nodes one may observe that for the Taylor flow the error decreases according to the assumed order of the scheme. Influence of

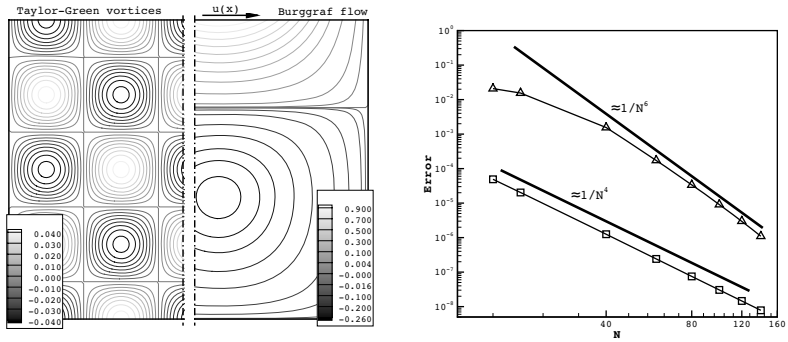

Fig. 1 Horizontal velocity component in the Taylor-Green flow and in the Burggraf flow (left figure) - CD results. Error of the horizontal velocity component in Taylor-Green flow (line with triangles) and in the Burggraf flow (line with squares).

the boundary closure is seen in the case of the Burggraf flow for which the solution accuracy decreases to 4th order.

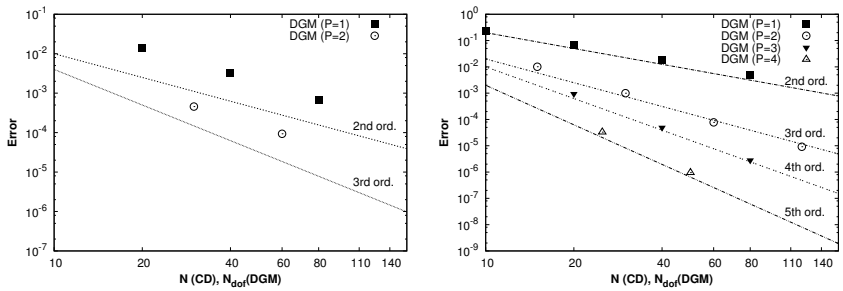

Fig. 2 Error of the horizontal velocity component for the Burggraf flow (left figure) and Taylor-Green flow. Number of degrees of freedom $N_{dof} = N_{el}^{x}(P+1)$, N_{el}^{x} – number of elements in one direction.

The results obtained with discontinous Galerkin method indicate that for Burggraf flow the method is only second order accurate, even when the order of expansion P is larger than one. The error decay is presented in Fig. 2. The reduction of order of accuracy for this particular flow is known in the literature and probably is related to the specific type of projection method used in the implementation of DGM. Reduction of the order has not been observed in CD code, using somewhat different procedure in projection step. In the case of Taylor vortices, the order of accuracy agrees with expectations, i.e. it equals $P+1$. It should be noticed, that for high order expansion DGM offers better accuracy than CD of the same number of degrees of freedom.

3.2 Temporal shear layer flow

The temporal shear layer flow is relatively simple example of turbulent flow, it was often used as the test case for the numerical codes for Direct and Large Eddy Simulation [7, 9, 11, 12]. The velocity profile is defined as $u(y) = Uerf(y\pi^{1/2})$. The Reynolds number defined as: $Re = U\delta/\nu$ (U – free stream velocity, δ – initial width of shear layer, ν – viscosity) was equal 250. In the computations with CD method the mesh consisted of 128×128 uniformly distributed nodes. The evolution of the shear layer (vorticity isocontours) is presented in Fig. 3, details of the flow characteristics may be found in [7, 9]. In this paper we concentrate on the comparison of the amplitudes of the most unstable mode and its subharmonic. The length of the computational domain L was equal four times the length of the most unstable mode (equal to 2.32π [9]), allowing to form four vortices corresponding to the most unstable mode which then was pairing due to the presence of the subharmonic modes.

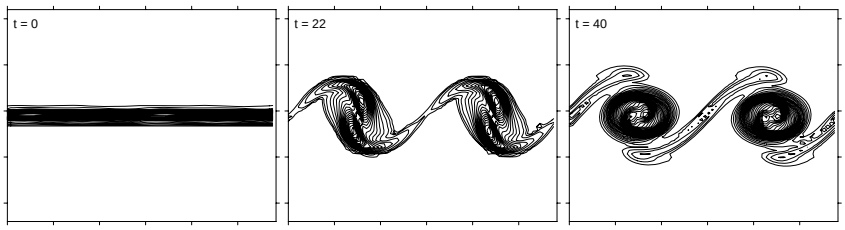

Fig. 3 Evolution of shear layer (vorticity isocontours).

The amplitudes of a given mode of the initial perturbation or in the evolved field are measured by the integrated RMS of the velocity modes defined as:

$$A_\alpha = \left[\int_{-L/2}^{+L/2} 2\hat{u}_x(\alpha)\hat{u}_x^*(\alpha)dy \right]^{\frac{1}{2}} \tag{2}$$

where $\hat{u}_i(\alpha)$ – Fourier coefficient of velocity component u_x and $\hat{u}_x^*(\alpha)$ – its complex conjugate. The evolution of the most unstable mode A_1 and its subharmonic $A_{1/2}$ are shown in Fig. 4. It can be observed the agreement between DGM and CD results is satisfactory only when the number of degrees of freedom in DGM is at least the same as the number of gridpoints in CD, although for the subharmonic mode reasonable accuracy is obtained even for quite coarse mesh (20×20, $P = 2$). This is not surprising, as the characteristic spatial scales related to that mode are much larger than for the most unstable mode. Both codes provide correct moment of time in which the maximum of the mode A_1 is attained [7, 9].

The support for the research was provided within the research grant WZ-1-101-701/2008 founded by Polish Ministry of Science and the statutory funds BS-1-103-301/2004/P. The authors are grateful to the Cyfronet and TASK Computational Center for access to the computing resources.

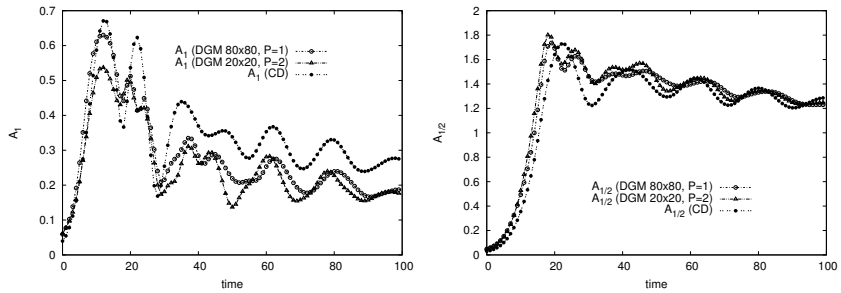

Fig. 4 Evolution of the most unstable mode (left figure) and its subharmonic (right figure)) .

References

1. Canuto C., Hussaini M.Y., Quarteroni A., & Zang T.A.: Spectral methods in fluid dynamics, Springer-Verlag, 1988
2. Cockburn B., Shu C-W.: Runge-Kutta Discontinuous Galerkin Methods for convection-dominated problems, Jounral of Scientific Computing, Vol.16, No.3, 2001
3. Fletcher C.A.J.: Computational Techniques for Fluid Dynamics, Springer-Verlag, 1991
4. Karniadakis G.E., Sherwin S.J.: Spectral/hp Element Methods for Computational Fluid Dynamics, Oxford University Press, 2005
5. Laizet S., Lamballais E.: High-order compact schemes for incompressible flows: A simple and efficient method with quasi-spectral accuracy, J. of Comput. Phys., vol. 228, pp. 5989?6015, 2009
6. Lele S.K.: Compact finite difference with spectral-like resolution. J. Comput. Phys., vol. 103, pp.16-42, 1992
7. Lesieur M., Staquet C., LeRoy P., Compte P.: The mixing layer and its coherence examined from the point of view of two-dimensionla turbulence J. Fluid Mech. Vol. 192, pp.511-534, 1988
8. Li, B.Q.: Discontinuous Finite Elements in Fluid Dynamics and Heat Transfer, Springer-Verlag, 2006
9. Moser D.R., Rogers M.M.: The three-dimensional evolution of plane mixing layer: pairing and transition to turbulence, J. Fluid Mech., vol. 247, pp. 275-320, 1993
10. Nagarajan S., Lele S.K., Ferziger J.H: A robust high-order compact method for large eddy simulation, J. of Comput. Phys., vol. 19 pp.392?419, 2003
11. Tyliszczak A.: Influence of the compact explicit filtering method on the perturbation growth in temporal shear-layer flow, Journal of Theoretical and Applied Mechanics, vol. 41, pp. 19-32, 2003
12. Vreman B., Geurts B., Kuerten H.: On the formulation of the dynamic mixed subgrid-scale model, Physics of Fluids, vol. 6, pp. 40-57, 1994

On the boundary treatment for the compressible Navier-Stokes equations using high-order discontinuous Galerkin Methods

Andreas Richter and Jörg Stiller

Abstract An appropriate boundary treatment is one of the most important tasks to perform when carrying out numerical simulations. The technique to define the boundary condition depends strongly on both the numerical scheme and the type of differential equation to be solved. In terms of implementation effort and cost of computational resources, every boundary should be treated locally in both space and time. In this paper we discuss techniques to deal with adiabatic walls in the framework of high-order discontinuous Galerkin methods for compressible flow.

1 Introduction

The treatment of boundaries is essential for the numerical simulation of fluid mechanics problems. A multitude of requirements exist: **i**) Stability and robustness. **ii**) The boundary condition has to reflect the physical problem, e. g. Dirichlét conditions and Neumann conditions. **iii**) The formulation should be local in space and time. **iv**) The boundary treatment has to respect the numerical scheme, e. g. the representation of curved walls has to be of the same order as the underlying scheme. **v**) The implementation has to fulfill the requirements listed above without an unrealistic expansion of the computational domain. Because there are so many requirements, it is difficult to find a general solution.

For the investigation of aeroacoustic problems as well as musical woodwind instruments we use a high-order discontinuous Galerkin finite element method in conjunction with a TVD Runge-Kutta time integration scheme to solve the unsteady and compressible Navier-Stokes equations in the form

Andreas Richter
Technische Universität Dresden, Institute for Aerospace Engineering, 01062 Dresden, Germany
andreas.richter4@tu-dresden.de

Jörg Stiller
Technische Universität Dresden, Institute for Fluid Mechanics, 01062 Dresden, Germany
joerg.stiller@tu-dresden.de

$$\partial_t \mathbf{U} + \nabla \cdot \vec{\mathbf{F}}(\mathbf{U}) = \nabla \cdot \vec{\mathbf{D}}(\mathbf{\Pi}, \nabla \mathbf{\Pi}),$$

with $\mathbf{U} = (\rho,\ \rho\vec{v},\ \rho e_t)^{\mathrm{T}}$ the solution vector and $\mathbf{\Pi} = (\vec{v},\ T)^{\mathrm{T}}$ the vector of primitive variables. To solve the diffusive terms an interior penalty scheme is used (Stiller et al., 2007; Richter et al., 2007, 2008, 2010; Hartmann and Houston, 2008). This leads to the weak form

$$\begin{aligned}
&\int_{\Omega_e} \Big(v_e \partial_t \mathbf{U}_e \,\mathrm{d}\Omega_e - \nabla v_e \cdot \Big(\vec{\mathbf{F}}(\mathbf{U}_e) - \vec{\mathbf{D}}(\mathbf{\Pi}_e, \nabla \mathbf{\Pi}_e) \Big) \mathrm{d}\Omega_e \Big) \\
&+ \int_{\Gamma_e} v_e \Big(\mathbf{H}_c(\mathbf{U}_e^{\pm}, \vec{n}) + \mathbf{H}_d(\{\mathbf{\Pi}_e\}, \{\nabla \mathbf{\Pi}_e\}, \mathbf{\Pi}_e^{\pm}, \vec{n}) \Big) \mathrm{d}\Gamma_e \\
&- \frac{1}{2} \int_{\Gamma_e} \nabla v_e \cdot \vec{\mathbf{C}}_n(\mathbf{U}_e^{-}) \Big(\mathbf{\Pi}_e^{-} - \mathbf{\Pi}_e^{+} \Big) \mathrm{d}\Gamma_e = 0 \quad (\text{for } \forall v_e \in \mathscr{V}_e \text{ and } \forall \Omega_e)
\end{aligned} \tag{1}$$

$$\vec{\mathbf{D}}(\mathbf{\Pi}, \nabla \mathbf{\Pi}) = \mathbf{C}(\mathbf{\Pi}) \cdot \nabla \mathbf{\Pi}$$

$$\mathbf{H}_d = \vec{n} \cdot \Big\{ \vec{\mathbf{D}} \Big\} + \frac{c_{ip}}{\Delta} \{\mathbf{C}_{nn}\} (\mathbf{\Pi}^{+} - \mathbf{\Pi}^{-})$$

with v_e the test function, $\mathbf{H}_c$ the convective and $\mathbf{H}_d$ the diffusive fluxes at the element boundaries Γ_e. The averages and jumps are defined as follows:

$$\{q\} = \frac{1}{2}(q^{-} + q^{+});\ \{\vec{q}\} = \frac{1}{2}(\vec{q}^{\,-} + \vec{q}^{\,+})$$

$$[\![q]\!] = \vec{n}(q^{-} - q^{+});\ \ [\![q]\!] = \vec{n} \cdot (\vec{q}^{\,-} - \vec{q}^{\,+}),$$

using $\{\}^{-}$ to denote values coming from the element interior and $\{\}^{+}$ for values from the outside. The convective and diffusive fluxes and the derivatives of the primitive variables need an appropriate treatment. Different strategies exist:

1. Hard correction of the solution field. This approach strictly keeps the boundary value but leads to instabilities, because it does not respect the type of the underlying differential equation.
2. Direct definition. This is only possible if the exact flux is known, e. g. at walls.
3. Alternatively, the outer values at the corresponding edge can be defined in such way that the resulting numerical flux meets the exact flux.
4. Characteristic treatment. Following Hirsch (1990) or Polifke et al. (2006), the solution can be divided into variables that propagate along characteristic directions. This quasi one-dimensional approach respects the hyperbolic character of the differential equation, but may fail at more complex geometries.
5. Puffer zone techniques such as Perfectly Matched Layers (PML) extend the computational domain by additional zones, in which the solution is damped to a homogeneous mean flow.

Depending on the boundary type, one of the strategies can be a good choice. For convective and diffusive fluxes, a combination of the listed strategies or a different

strategy altogether may be useful or necessary. In this contribution we focus on adiabatic walls. We shall discuss inflows and outflows in further publications.

2 Treatment of adiabatic, full-reflective walls

2.1 Advective flux treatment

In terms of adiabatic and hard walls, the characteristic formulation reads

$$\frac{Z_1^{new} - Z_1^{old}}{\Delta t} = \Delta_t Z_1 = \frac{1}{\rho a}\Delta_t p^{corr} - \Delta_t v_n^{bc} \stackrel{!}{=} \Delta_t Z_4 = \frac{1}{\rho a}\Delta_t p + \Delta_t v_n \,,$$

with $\Delta_t \mathbf{Z} = \Delta t \mathbf{R}^{-1}\dot{\mathbf{U}}$. It describes the reflection of characteristics running outwards. This formulation requires time derivatives of both the pressure and velocity, which are typically determined by linearization. Because this linearization can produce oscillations that disturb the solution, this strategy shall not be pursued further. At stationary walls the boundary flux can be prescribed directly with

$$\mathbf{H}_{bc} = \begin{pmatrix} 0 \\ p^- \vec{n} \\ 0 \end{pmatrix} ,$$

or alternatively it can be constructed by mirroring the outer state to fit the boundary flux

$$\mathbf{U}^+ = \begin{pmatrix} \rho^- \\ \vec{v} - \alpha_1 \vec{n} v_n \\ \rho e_t^- + \beta_1 e_{kin}^- \end{pmatrix} \quad \alpha_1 = 1\ldots 2,\ \beta_1 = -1\ldots 1\,. \tag{2}$$

For frictionless systems –like solutions of the Eulerian equation– the outer total energy state fully accounts for the inner energy. For systems with friction, different choices for the kinetic energy are possible.

2.2 Diffusive flux treatment

The characteristic formula to treat the diffuse flux is also based on time linearization and is therefor not discussed here. As the velocity gradients are unknown at the wall, only an incomplete data set to define the exact diffusive flux is given. Alternatively the outer state can be constructed by setting the velocity field to zero or by mirroring the velocity. The outer temperature has to meet the inner temperature because no temperature gradients are allowed. The constructions scheme follows

$$\mathbf{\Pi}^+ = \begin{pmatrix} \vec{v}^- - \alpha_2 \vec{v}^- \\ T^- \end{pmatrix},$$

with α_2 equal to one in terms of setting the velocity to the boundary value, or two for mirroring.

2.3 Gradients

Gradients can be treated similarly as diffusive fluxes. Only the temperature gradient is given to construct the outer state, while the wall shear stress is unknown. This leads to

$$\begin{aligned} (\nabla \vec{v})^+ &= (\nabla \vec{v})^- \\ \partial_n T^+ &= \partial_n T^- - \beta_3 \partial_n T^- , \end{aligned}$$

with β_3 also a constant value between one and two.

3 Test case

As test case, a lid-driven cavity is investigated in two steps: First the flow is driven by a moving isothermal wall on the top. Then, all walls are defined stationary and adiabatic and the development of the mass and the total energy inside the container and also the temperature gradients at the boundaries are measured. The domain is divided into 4 x 4 elements of polynomial order 8, the Reynolds number during the start up process is 400 (Fig. 1).

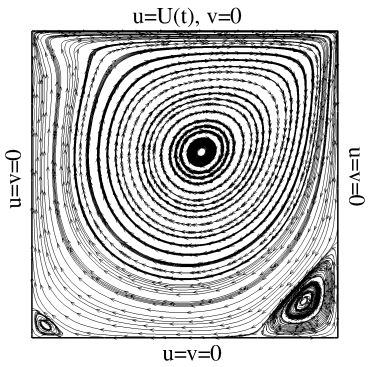

Fig. 1 Lid-driven cavity. Snapshot of flow field.

4 Mass conservation

Tab. 1 displays mass conservation as function of advective flux treatment. Two results emerge: Firstly, a factor $\beta_1 \neq 0$ in Eq. 2 significantly reduces the conservation properties. They also deteriorate when the outer normal velocity is set to zero instead of mirroring it. On the other hand, neither the treatment of diffusive fluxes nor that of velocity and temperature gradients influences mass conservation measurably.

Table 1 Mass conservation as function of adiabatic fluxes*.

advective flux treatment		L^∞ norm of mass error
$\mathbf{H} = \mathbf{H}_{bc}$		$7.320 \cdot 10^{-12}$
$v_n^+ = -v_n^-$	$\rho e_t^+ = \rho e_t^- + e_{kin}^-$	$8.301 \cdot 10^{-9}$
$v_n^+ = -v_n^-$	$\rho e_t^+ = \rho e_t^- - e_{kin}^-$	$8.286 \cdot 10^{-9}$
$v_n^+ = -v_n^-$	$\rho e_t^+ = \rho e_t^-$	$7.320 \cdot 10^{-12}$
$v_n^+ = 0$	$\rho e_t^+ = \rho e_t^- + e_{kin}^-$	$5.606 \cdot 10^{-7}$
$v_n^+ = 0$	$\rho e_t^+ = \rho e_t^- - e_{kin}^-$	$4.099 \cdot 10^{-7}$
$v_n^+ = 0$	$\rho e_t^+ = \rho e_t^-$	$4.852 \cdot 10^{-7}$

*Diffusive fluxes equivalent to the first row in Tab. 2.

5 Total energy conservation

The other hand the total energy strongly depends on the treatment of the diffusive terms. For reasons of mass conservation the energy correction term $\pm e_{kin}$ drops and the remaining choices of the advective flux have no effects on the total energy. Interestingly, uncoupled variations of both the diffusive flux and the primitive variable gradients seem to have no effect on the energy losses. Only one configuration –the combination of mirrored temperature gradients and mirrored velocities– pushes the energy losses two orders downward.

Table 2 Total energy conservation as function of primitive variables and their gradients*.

diffusive flux treatment		gradients		L^∞ norm of total energy error
$\vec{v}^+ = 0$	$T^+ - T^-$	$\partial_n T^+ = 0$	$(\nabla \mathbf{v})^+ = (\nabla \mathbf{v})^-$	$1.628 \cdot 10^{-6}$
$\vec{v}^+ = 0$	$T^+ - T^-$	$\partial_n T^+ = -\partial_n T^-$	$(\nabla \mathbf{v})^+ = (\nabla \mathbf{v})^-$	$4.443 \cdot 10^{-6}$
$\vec{v}^+ = -\vec{v}^-$	$T^+ - T^-$	$\partial_n T^+ = 0$	$(\nabla \mathbf{v})^+ = (\nabla \mathbf{v})^-$	$9.818 \cdot 10^{-6}$
$\vec{v}^+ = -\vec{v}^-$	$T^+ - T^-$	$\partial_n T^+ = -\partial_n T^-$	$(\nabla \mathbf{v})^+ = (\nabla \mathbf{v})^-$	$7.844 \cdot 10^{-8}$

*Advective flux $\mathbf{H} = \mathbf{H}_{bc}$.

6 Conclusion

In this article we present results of the study of different techniques to define adiabatic hard walls in the framework of high-order discontinuous Galerkin schemes. In these, mass conservation depends strongly on the exact definition of the advective flux, while energy conservation is guaranteed only if both the primitive variables and their gradients are properly defined. In general, mirroring all values may be a good choice for fluxes that cannot be calculated directly.

Acknowledgements This work was supported by the German National Science Foundation (Deutsche Forschungsgemeinschaft, DFG) within the project *Numerical simulation of the sound spectrum and the sound radiation in and around a recorder* (*Numerische Simulation des Klangspektrums und der Schallausbreitung in und um eine Blockflöte*).

References

Hartmann, R. and Houston, P. (2008). An optimal order interior penalty discontinuous Galerkin discretization of the compressible Navier-Stokes equations. *Journal of Computational Physics*, 227(22):9670–9685.

Hirsch, C. (1990). *Numerical Computation of Internal and External Flows Vol. 1 & 2*. Wiley-Interscience Publication.

Polifke, W., Wall, C., and Moin, P. (2006). Partially reflecting and non-reflecting boundary conditions for simulation of compressible viscous flow. 213:437–449.

Richter, A., Brußies, E., Stiller, J., and Grundmann, R. (2010). Aeroacoustic investigation of woodwind instruments based on discontinuous Galerkin methods. In: *Computational Fluid Dynamics Review 2010*, World Scientific Publishing Company, Inc..

Richter, A., Stiller, J., and Grundmann, R. (2007). Stabilized discontinuous Galerkin methods for flow-sound interaction. *Journal of Computational Acoustics*, 15(1):123–143.

Richter, A., Stiller, J., and Grundmann, R. (2008). Stabilized high-order discontinuous Galerkin methods for aeroacoustic investigations. *ICCFD 2008, Seoul*.

Stiller, J., Richter, A., and Brußies, E. (2007). A physically motivated discontinuous galerkin method for the compressible navier-stokes equations. *ICOSAHOM 2007, Beijing*.

Analytical and numerical investigation of the influence of artificial viscosity in Discontinuous Galerkin methods on an adjoint-based error estimator

Jochen Schütz, Georg May and Sebastian Noelle

Abstract Recently, it has been observed that the standard approximation to the dual solution in a scalar finite difference context can actually fail if the underlying forward solution is not smooth [9]. To circumvent this, it has been proposed to over-refine shock structures of the primal solution. We give evidence that this is also the case in the discontinuous Galerkin approach for the one-dimensional Euler equations if one explicitely adds diffusion. Despite this, on the first sight very negative result, we demonstrate that, if using the dual solution only for adaptation purposes, a special treatment seems not to be necessary to get good convergence in terms of a target functional.

1 Introduction

1.1 Background

Distributing degrees of freedom economically in the numerical computation of hyperbolic conservation laws has motivated the development of error control.

Traditionally, e.g. in the context of elliptic equations, one has always tried to reduce the solution error in some given norm below some given treshold, i.e. the approach *take as little degrees of freedom as possible to achieve* $\|w - w_h\| < \varepsilon$, where w is the exact and w_h the approximated solution (see e.g. [10] for a good overview).

Jochen Schütz, Georg May
AICES Institute for Advanced Study in Computation Engineering Science, RWTH Aachen University, Schinkelstr. 2, 52062 Aachen, e-mail: lastname@aices.rwth-aachen.de
Sebastian Noelle
IGPM, RWTH Aachen University, Templergraben 55, 52062 Aachen, e-mail: noelle@igpm.rwth-aachen.de

In engineering applications, however, one is often interested in only one or a few single numbers coming from the solution w, e.g. in aerodynamics these numbers could be lift or drag. Mathematically speaking, one is interested in $J(w)$, where J is a given, probably nonlinear functional (usually called *target functional*). This has motivated the aproach *take as little degrees of freedom as possible to achieve* $|J(w) - J(w_h)| < \varepsilon$. This error can be approximately calculated via the adjoint method.

A lot of work has been put into the development and theoretical justification of adjoint methods supposed that the underlying solution is smooth ([4], [8]). Despite its importance for the use in the context of hyperbolic conservation laws, only a few publications have been concerned with the correct adjoint formulation in the case where there is a jump discontinuity in the underlying forward solution, see e.g. [3], [9], [13] and the references therein.

Recently, it has been observed that the discrete approximation to the dual can actually fail ([7], [9]) in the case of a shock in the underlying forward solution. The key observation of the authors of the aforementioned paper is that the loss of information within the discontinuity is too much to allow for giving precise initial data of the gradient of the objective function.

To circumvent this feature, the authors in [9] have proposed (and, for their very special setting, also proved) that an over-refinement of the shock-structure, i.e. giving viscosity of $O(h^\alpha)$, where h is the cell-size and $\alpha < 1$, does lead to convergent adjoint solutions.

We have been conducting experiments and came to the conclusion that this does also hold for the case when one approximates the one-dimensional steady-state Euler equation with a DG method - stabilized by explicit artificial diffusion - so, as expected, it is not a particular feature of the approach of [7] and [9]. We will demonstrate these findings and investigate how they influence an adaptation algorithm.

1.2 Underlying primal equation

We will in the course of this paper consider a one-dimensional model problem; the quasi one-dimensional steady Euler nozzle flow with flux f and sourceterm S ([1]) through a convergent-divergent duct of given geometry $A(x)$ ($x \in \Omega \subset \mathbb{R}$).

1.3 Adaptive DG discretization with artificial diffusion

We discretize our primal equations by using a Discontinuous Galerkin method (cf. [5], [2]). In the last few years, these methods have gained quite a lot of attention, as they bring together the advantages of Finite Element methods (the built-in high-order) and the advantages of Finite Volume methods (the stability due to upwinding). Furthermore, even in the very high order context, DG methods stay local which makes them very well suited for parallel computations.

Recently, several authors (e.g. [12], [6]) have suggested to explicitely add artificial, solution-dependent diffusion terms for stabilization into the method.
We discretize the convective term with the approach of Cockburn and Shu [5], while for the viscous term, we use a Bassi-Rebay 2 discretization [2].

We modify the treatment of the boundary conditions in such a way that our discretization is asymptotically adjoint consistent (cf. [2], [11]). In our adaptation procedure, we start with a rather coarse grid and calculate a primal solution w_h^1. We then calculate a dual error estimator (see next section) which drives the adaptation algorithm. To avoid 'extremal' refinement steps (like e.g. refine only one cell, or refine all), we use the so-called *fixed-fraction criterium* ([4]) which refines a fixed fraction q of cells that have the largest error indicator.

2 Linearization and dual equation

We are mainly interested in variations of J, i.e. (directional) gradients of the functional $J(w) := \int_\Omega p(w)\ dx$. We will for simplicity in this section only deal with the one-dimensional model problem (for more sophisticated cases, we refer to [3] and the references therein), where its solution is assumed to have a discontinuity at $x = \alpha$.

Given a function v that is supposed to fulfill the *dual equation*

$$-f'(w)^T v_x + S'(w)^T v = p'(w) \qquad \forall x \in \Omega \tag{1}$$

$$v^T f'(w)\xi = 0 \qquad \forall x \in \partial\Omega, \forall \xi \in Ker(B'(w)), \tag{2}$$

$$v_2(\alpha) = -\frac{A(\alpha)}{A'(\alpha)} \tag{3}$$

and that is additionally supposed to be continuous at $x = \alpha$, we end up with the fact that the linearization can be written as

$$J'(w)\overline{w} = \int_\Omega v^T \cdot \left((f'(w)\overline{w})_x + S'(w)\overline{w} \right)\ dx. \tag{4}$$

Of course the internal boundary condition (3) is awkward in actual numerical calculations for several reasons, one being the uncertainty about α. This is why most authors do not at all consider this internal boundary condition but just calculate a solution to (1)-(2) in the hope of reaching (3) for free. This has been very successful in the context of low-order methods (cf. [8], [14]), although Giles published, for the time-dependent scalar case, a simple counter example (cf. [7]).

3 Numerical results

The h^α viscosity approach: As mentioned in the introduction, the convergence towards the dual solution can actually fail unless one gives enough diffusion ([7], [9]). We have - in the 1D Euler case - been conducting experiments and have found out that this is also true in our setting.

Let us consider a one-dimensional test-case with a free-stream Mach number of 0.5 and an exit pressure of $p_{out} = 1.0$. For our smooth geometry, this creates a shock at position $x = 5.25...$ (which can, thanks to the explicit solution, be calculated in advance). Both primal and dual solution are calculated with polynomial order once $p = 1$ and once $p = 3$ on the same mesh.

To demonstrate our findings, we assume that the viscosity $\varepsilon(w) \equiv \varepsilon$ is constant throughout our domain Ω. As a measure of error, we use the relative deviation of the dual solution v in fulfilling (3). Figure 1 plots the amount of viscosity used versus the error in the dual solution.

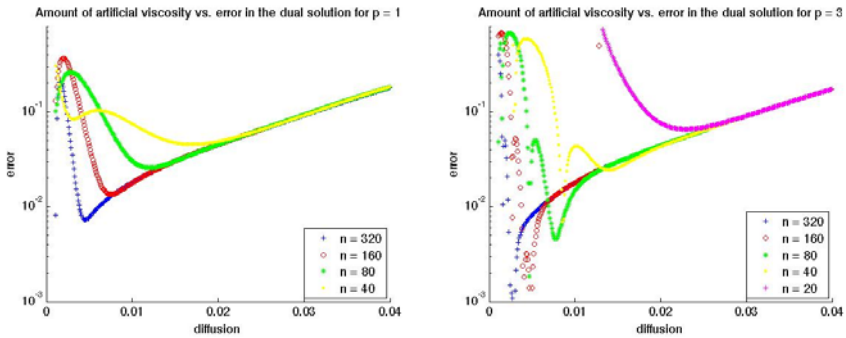

Fig. 1
Amount of artificial viscosity versus error in the adjoint solution for $p = 1$ and $p = 3$.

There are some remarks in order about the plot: Notice the right hand side where all the graphs lie above each other. This means that both primal and dual solution are perfectly grid-converged and that the only source of error stems from the viscosity term. The interesting point is always when the graphs 'leave' the common region (on the left hand side of the plot) because this is where discretization errors begin to dominate the overall error. What can be seen is that these occurences do not appear linearly with respect to the mesh-size but that they eventually occur earlier and earlier.

These findings motivate the conclusion that one shoud take viscosity constant to h^α, where α is slightly less than unity, to ultimately guarantee convergence of the adjoint solution.

We demonstrate the advantage in taking the viscosity proportional to $h^{0.8}$ in Figure 2. When giving viscosity proportional to h, the dual solution does not converge

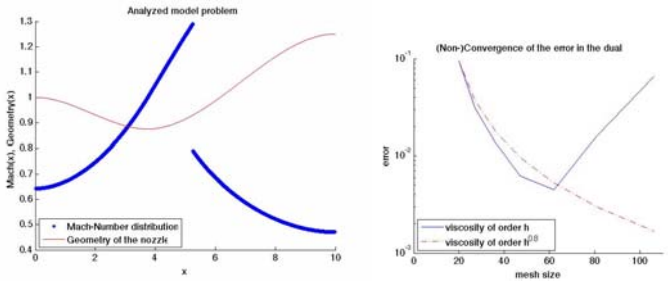

Fig. 2
Plot of the model problem and convergence history of the adjoint solution for $p = 3$.

at all, while when adding diffusion as $O(h^{0.8})$, we have a perfectly acceptable convergence history.

What one can also see when comparing the two pictures in Figure 1 is that the higher-order solution needs a little less (about half) the amount of viscosity to accurately resolve the dual solution on the same mesh.

It remains to prove these findings similar to [9]. Unfortunately, this will be - due to the more complicated structur of the Euler equations - a non-trivial task as already mentioned in [9].

Adaptivity by the adjoint without enforcing the h^{α} approach: Despite the very negative results in the preceeding subchapter, we want to demonstrate that - for using adaptivity - it does not seem necessary at all to enforce the dual boundary condition.

Let us therefore look at Figure 3. We ran a test with the same starting parameters as the one for Fig. 2, with the difference that we now did not refine uniform, but we did refine where the adjoint error estimation did tell us to. The constant viscosity was chosen to be of size $O(h)$ and $O(h^{0.8})$, respectively, where h is the minimum mesh-size.

Of course we are not primarily interested in whether the adjoint internal boundary condition (3) does converge or whether not, but we are interested in how far the primal functional J converges. It can be seen clearly from Fig. 3, that even if the dual does not converge towards the boundary condition (and, in so far, the dual does not converge properly),we still get an adaptation criterion that seems to be very reasonable.

Note that, furthermore, due to the viscosity of size $O(h)$, the 'standard' approach which concerns viscosity seems to converge mush faster in terms of the functional J (which is - after all - not very surprising). The actual surprising part is that as an adaptation criterion, the standard approach seems to be as good as the over-refinement approach.

This in some way demonstrates the capability of the adjoint approach even if one does not enforce or even achieve the internal dual boundary condition (3). (This is what actually most authors do - just neglect (3). Our findings could justify their approach.)

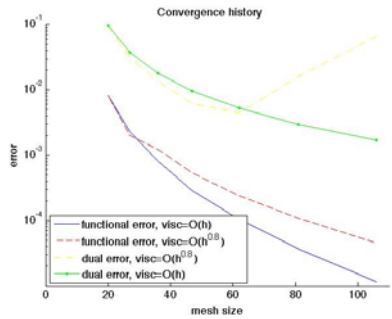

50mm

Fig. 3

Convergence history of the adjoint solution for $p = 3$.

Acknowledgements Financial support from the Deutsche Forschungsgemeinschaft (German Research Association) through grant GSC 111 is gratefully acknowledged.

References

1. Anderson, J. D.: Fundamentals of Aerodynamics. McGraw-Hill, (2001)
2. Arnold, D.N., Brezzi, F., Cockburn, B., Marini, D.L.: Unified analysis of discontinuous galerkin methods for elliptic problems. SIAM J. Numer. Anal, **39**, 1749–1779 (2002)
3. Bardos, C. and Pironneau, O.: Data assimilation for conservation laws. Methods and Applications of Analysis, **12**, 103-134 (2005)
4. Becker, R., Rannacher, R.: An optimal control approach to a posteriori error estimation in finite element methods. Acta Numerica, **10**, 1–102 (2001)
5. Cockburn, B., Shu, C-W.: The runge-kutta local projection p^1-discontinuous galerkin finite element method for scalar conservation laws. IMA Preprint, **388**, (1988)
6. Darmofal, D.L., Barter, G.: Shock capturing with higher-order, pde-based artificial viscosity. Proc. of the 18th AIAA CFD Conference, (2007)
7. Giles, M.: Discrete adjoint approximation with shocks. Proc. of the 9th International Conference on Hyperbolic Problems, (2002)
8. Giles, M., Pierce, N.: An introduction to the adjoint approach in design. Flow, Turbulence and Combustion, **65**, 393-415 (2000)
9. Giles, M., Ulbrich, S.: Convergence of linearised and adjoint approximations for discontinuous solutions of conservation laws. Technical Report TU Darmstadt and Oxford University, (2008)
10. Oden, J.T., Ainsworth, M.: A posteriori error estimation in finite element analysis. Comput. Methods Appl. Mech. Engrg., **142**, 1–88 (1997)
11. Oliver, T.A., Darmofal, D.L.: Analysis of dual consistency for discontinuous galerkin discretizations of source terms. SIAM J. Numer. Anal, (2008)
12. Persson, P.-O., Peraire, J.: Sub-cell shock capturing for discontinuous galerkin methods. Proc. of the 44th AIAA Aerospace Sciences Meeting and Exhibit, (2006)
13. Ulbrich, S.: Optimal control of nonlinear hyperbolic conservation laws with source terms. Technical Report TU München, (2001)
14. Venditti, D.A., Darmofal, D.L.: Adjoint error estimation and grid adaptation for functional outputs: Application to quasi-one-dimensional flow. Journal of Computational Physics, **164**, 204–227 (2000)